THE JOURNAL OF PHYSICAL CHEMISTRY C

Article

pubs.acs.org/JPCC

Validation of Capillarity Theory at the Nanometer Scale by Atomistic Computer Simulations of Water Droplets and Bridges in Contact with Hydrophobic and Hydrophilic Surfaces

Nicolas Giovambattista,[*,†,‡] Alexandre B. Almeida,[§,∥] Adriano M. Alencar,[∥] and Sergey V. Buldyrev[§]

[†]Department of Physics, Brooklyn College of the City University of New York, Brooklyn, New York 11210, United States

[‡]Ph.D. Programs in Chemistry and Physics, The Graduate Center of the City University of New York, New York, New York 10016, United States

[§]Department of Physics, Yeshiva University, 500 West 185th Street, New York, New York 10033, United States

[∥]Instituto de Física, Universidade de São Paulo, 05508-090, São Paulo, SP, Brazil

ABSTRACT: Capillarity is the study of interfaces between two immiscible liquids or between a liquid and a vapor. The theory of capillarity was created in the early 1800s, and it is applicable to mesoscopic and macroscopic (>1 μm) systems. In general, macroscopic theories are expected to fail at the <10 nm scales where molecular details may become relevant. In this work, we show that, surprisingly, capillarity theory (CT) provides satisfactory predictions at 2−10 nm scales. Specifically, we perform atomistic molecular dynamics (MD) simulations of water droplets and capillary bridges of different symmetry in contact with various surfaces. The underlying structure of the surfaces corresponds to hydroxilated (crystalline) silica which is modified to cover a wide range of hydrophobicity/hydrophilicity. In agreement with CT, it is found that water contact angle is independent of the droplet/bridge geometry and depends only on the hydrophobicity/hydrophilicity of the surface employed. In addition, CT provides the correct droplet/bridge profile for all (hydrophobic/hydrophilic) surfaces considered. Remarkably, CT works even for the very small droplets/bridges studied, for which the smallest dimension is ≈2 nm. It follows that the concepts of surface tension and contact angle are indeed meaningful at 2−10 nm scales even when, macroscopically, such concepts are not justified. In order to confirm the self-consistency of CT at 2−10 nm scales, we also calculate the capillary forces between different surfaces induced by water capillary bridges. These forces depend on the liquid−vapor surface tension of water, γ. Using CT, the calculated forces indicate that $\gamma = 0.054 \pm 0.001$ N/m^2. This is in agreement with the value $\gamma = 0.056 \pm 0.001$ N/m^2 obtained independently using the Kirkwood−Buff method, and it is consistent with values of γ reported in the literature for the present water model. Confirming the validity of CT at 2−10 nm scales has relevant implications in scientific applications, such as in our understanding of self-assembly processes at interfaces. We discuss briefly this and other consequences of the present results.

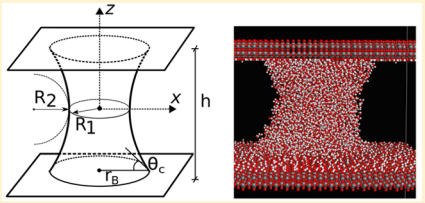

I. INTRODUCTION

Capillarity is the study of deformable interfaces formed between a liquid and a vapor or between immiscible liquids.[1] Examples of capillarity phenomena are abundant. For example, it is the formation of water bridges (capillary bridges) between grains of sands that allows sand castles to stand still.[2] In biology, e.g., capillarity phenomena allow insects to "walk" on water[3] and provide insects with adhesion pads in their legs to attach to surfaces.[4,5] In medicine, capillary bridges may form during inflammatory processes of lungs.[6,7] Capillarity plays a major role in diverse technological and scientific applications, such as in soil science and climate as well as in textiles production and the treatment of glass surfaces.[1]

The field of capillarity was developed in the early 19th century by Laplace and Young.[1] The classical theory of capillarity is well-developed and is based on the concept of surface tension. Capillarity theory (CT) is a macroscopic approach applicable to liquid volumes in the >1 μm scales. Extending CT to the nanoscale is desirable partially due to its relevance in scientific and technological applications.[8] For example, humidity can induce the formation of capillary bridges of nanoscale dimensions between the tip of atomic force microscopes (AFM) and the surface of interest.[9−11] Such nanoscale liquid bridges may affect AFM measurements,[12,13] and quantifying such capillary bridge forces is hence necessary. Similar liquid bridges play relevant roles in "dip pen" nanolithografy techniques,[14] industrial processes such as sintering,[15] and ink transfer processes in contact printers.[16−18]

As the typical length scale is reduced below 100 nm, deviations from CT are expected, particularly at <10 nm scales where molecular details become relevant. Remarkably, computer simulation studies of <10 nm size droplets are consistent with macroscopic predictions of CT; for example, these studies show that the average profile of nanoscale droplets is indeed spherical (as predicted by CT) (see, e.g., refs 19−21). Similarly, detailed studies of nanoparticles immersed in a liquid

Received: October 23, 2015
Revised: December 15, 2015
Published: December 31, 2015

DOI: 10.1021/acs.jpcc.5b10377
J. Phys. Chem. C 2016, 120, 1597−1608

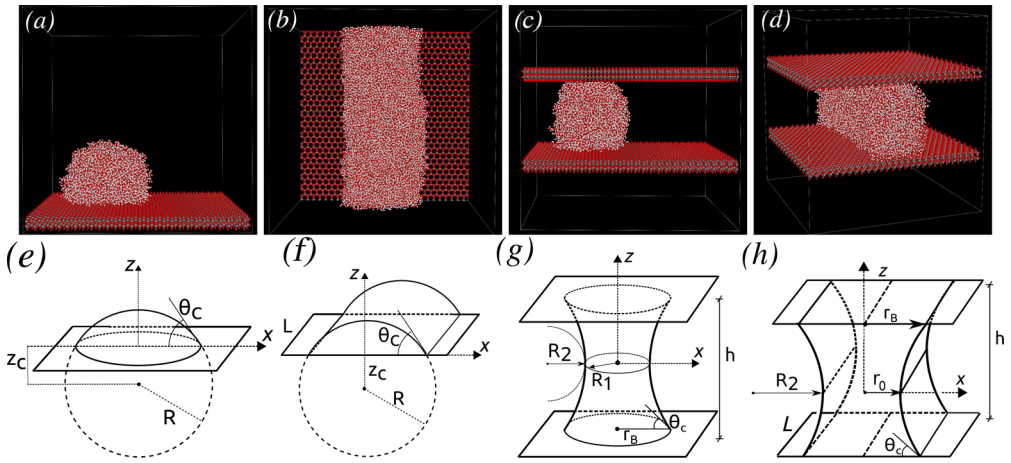

Figure 1. Snapshots from computer simulations of (a) AS droplet (side view), (b) TS droplet (top view), (c) AS bridge (side view), and (d) TS bridge (side view) for hydrophobic surfaces with surface polarity $k = 0.0$. Panels e, f, g, and h are, respectively, the schematic diagrams indicating the relevant parameters used in the present work for each of the systems in (a), (b), (c), and (d) (see text).

and vapor phase show that the solvent-mediated interactions between (≈ 2 nm size) particles are consistent with CT.[22] We note that theoretical and computer simulation studies show that CT can be used to describe accurately the adsorption behavior of nonspherical nanoparticles at liquid−liquid interfaces.[23,24] Many of these computational studies are based on idealized liquids and/or surfaces where, for example, the liquid and/or surfaces are composed of Lennard-Jones particles (see, e.g., ref 25). Yet, computer simulations show that expressions obtained from CT, in general, hold at the nanoscale. In a different context, macroscopic thermodynamics has been applied successfully to study nanoconfined fluids.[26−28] However, in many of these cases, the expressions from CT are employed to fit simulation data using quantities, such as surface tensions, as free fitting parameters. In other cases, successful application of CT to describe nanoscale systems requires additional concepts, such as line tension, which play no role at the *macro*scale (see, e.g., refs 19, 22, 24, and 29). In some situations, application of CT to small systems requires additional nontrivial approximations.[30] It follows that although expressions from CT may hold at the nanoscale, it is not evident whether the basic hypothesis of CT hold at nanometer-scale dimensions and, hence, whether the theory is self-consistent.

The goal of this work is to test whether the fundamental hypothesis of CT hold at the 2−10 nm scales. Specifically, macroscopic (>1 μm) CT assumes that (i) the surface tension of a given liquid (in contact with a another liquid, vapor, or solid) is universal, i.e., it is independent of the liquid interface geometry (e.g., liquid droplet vs liquid bridge), and (ii) the free energy of the system can be expressed solely in terms of the surface tensions of the liquid of interest (in contact with a vapor, solid, or other relevant phase), the geometry of the liquid interface, and the free energy of the bulk liquid. To test point i, we perform molecular dynamics (MD) simulations to study droplets and capillary bridges of <10 nm scale dimensions in contact with hydrophobic and hydrophilic surfaces. We use a realistic full-atomistic model system where the droplet/bridges are composed of water molecules and the walls correspond to hydroxilated silica (see section II.A). We find that CT predicts remarkably well the profiles of all the droplet/bridge studied. Remarkably, for a given surface, we recover the same liquid−vapor surface tension and water contact angles, confirming the validity of point i. To test point ii, we focus on the water capillary bridges between the *same* surfaces employed in point i and study the forces induced by the capillary bridges on the walls. These forces are simple derivatives of the system free energy. Remarkably, the forces obtained from simulations are in quantitative agreement with the predictions of CT. In particular, the relevant quantities that define these capillary forces, such as surface tension and contact angle, are in agreement with the corresponding values obtained in the studies of point i. Our results confirm that points i and ii hold quantitatively at 2−10 nm scales and, hence, that CT is self-consistent at such small dimensions.

This paper is structured as follows. In section II, we discuss the simulation details and, in particular, the methodology followed to calculate the droplet and bridge properties from both MD simulations and CT. Section III presents the main findings of this work, i.e., a detailed comparison of computer simulation results and the corresponding predictions from CT. A summary and discussion are included in section IV.

II. COMPUTER SIMULATIONS AND NUMERICAL METHODS

A. Simulation Details. Our findings are based on MD simulations of water nanodroplets and bridges in contact with surfaces of different hydrophobicity/hydrophilicity. We consider two kinds of droplets: axis symmetric (AS) and translationally symmetric (TS) (see Figure 1). The AS droplets are symmetric under rotations around the z-axis, which is perpendicular to the surface (see Figure 1a,e). The TS droplets are symmetric under translations along the y-axis[31] (see Figure 1b,f). In all cases, periodic boundary conditions are applied along the x-, y-, and z-axes, and the walls expand across the entire xy-plane. Similarly, we consider capillary bridges formed between parallel surfaces that are axis symmetric and translationally symmetric [see Figures 1c,g and 1d,h]. By considering TS droplets and TS bridges, we remove any effect due to (vapor−solid−liquid) line tensions that may play a relevant role in the case of nanoscale AS droplets/bridges (see, e.g., refs 19 and 32).

All simulations are performed for a cubic system of side length L, at constant volume, number of water molecules N, and temperature $T = 300$ K. Simulations are performed using the LAMMPS software package[33] with water molecules being represented by the SPC/E model.[34] Coulomb and Lennard-

DOI: 10.1021/acs.jpcc.5b10377
J. Phys. Chem. C 2016, 120, 1597−1608

Jones interactions are cut off at distance r_{cutoff} = 10 Å, and long-range electrostatic interactions are calculated using a particle−particle particle-mesh solver[35] with an accuracy value of 10^{-5}. The temperature is controlled using a Nosé−Hoover style thermostat employing the equations of motion described by Shinoda et al.[36] All simulations are run for 5 ns, and the last 2 ns of the simulation is used for data analysis.

In the case of AS droplets, we consider two system sizes: N = 3375 (L = 138.6 Å) and N = 6750 (L = 277.2 Å). This allows us to test for size effects in our calculations. AS bridges are composed of N = 3375 (L = 138.6 Å). In these cases, the starting water droplet/bridge configuration is a cubic configuration taken from an independent simulation of *bulk* water at ρ = 1 g/cm^3 and T = 300 K. The TS droplets and TS bridges are composed of N = 9897 molecules (L = 138.6 Å). In these cases, the starting water configuration is orthorhombic (obtained from an independent simulation of *bulk* water equilibrated at ρ = 1 g/cm^3 and T = 300 K) that extends across the system along the y-axis. In the case of bridges, the starting water configuration is sandwiched by two identical walls separated by a distance h = 50 Å, which is maintained constant during the whole simulation. We note that in all cases the starting configuration is not relevant since it takes a few picoseconds for the water molecules to reorganize in a spherical (AS droplet), cylindrical (TS droplets), or bridge-like geometry.

For each droplet and bridge system, we consider a family of walls that vary in the degree of hydrophobicity/hydrophilicity. These walls have been used previously and are described in detail in refs 37 and 38. Briefly, the wall structure corresponds to four layers of SiO_2, reproducing the (1, 1, 1) face of β-cristobalite. The walls are orthogonal to the z-axis, span the entire system, and are periodic along the x- and y-directions. The wall surface in contact with the water droplet/bridge is hydroxylated by attaching a hydrogen (H) atom to each surface oxygen. The Si and O atoms are fixed during the simulation, but the OH bonds, of fixed length 1 Å, are allowed to rotate in a plane parallel to the wall. In LAMMPS, this is done by fixing simultaneously the H−Si and H−O distances of the surface silanol groups (i.e., by fixing the distances of the H atom to the closest O and Si atoms). As a result, H and O atoms of the silanol groups are located in planes separated by $\Delta z \approx 0.33$ Å from each other. In all simulations we measure the distance to a given wall as the distance to the plane of the wall's H atoms.

All wall atoms, with the exception of the H atoms, interact with water via a Lennard-Jones potential. Only the Si, O, and H atoms of the surface silanol groups have a nonzero partial charge, and hence, they interact with water via Coulomb interactions. The wall structure, LJ parameters of the wall atoms, and the corresponding partial charges are provided in ref 38. In the hydroxylated silica surface, the silanol group partial charges are $q_{0,Si} = 0.31e$, $q_{0,O} = -0.71e$, and $q_{0,H} = 0.40e$ and the surface is hydrophilic, as expected. In order to vary the hydrophilicity of the surface, we follow ref 37 and rescale the silanol group partial charges by a factor $0 \le k \le 1$, i.e., $q_i \rightarrow k \times q_{0,i}$ where i = O, Si, and H. It can be easily shown that k is an adimensional factor that quantifies the surface polarity.[37]

In the case k = 1, one recovers the original hydroxylated silica walls. For k = 0 the surface is hydrophobic; surface atoms have no partial charges, and the H atoms effectively vanish since they have no interactions with water. In ref 37, it is shown that the surfaces are hydrophobic; i.e., the contact angle of SPC/E water is >90°, for approximately $k < 0.4$. We note that the simulations of ref 37 were performed using an in-house MD code, while the present simulations are performed using the LAMMPS package and simulations time scales are much longer. As shown below, the present results show that the contact angles of water in contact with the different surfaces studied are in agreement with the values reported originally in ref 37.

B. Methods and Numerical Calculations. In this section, we describe how the droplets/bridges profiles and density contour maps reported in this work are calculated from the MD simulations. We also describe the procedure followed to fit the MD simulation profiles using the corresponding equations from CT.

1. Droplet and Bridge Profiles from MD Simulations. For AS droplets and AS bridges, the corresponding profiles are built from 2000 snapshots obtained from the last 2 ns of the simulation and taken every 1 ps. For each snapshot, we first define a z-axis passing through the center of mass of the droplet/bridge, perpendicular to the wall(s). The droplet/bridge is then covered with overlapping slabs of thickness 5 Å parallel to the wall(s) and shifted vertically by 2.5 Å with respect to each other. For each slab, centered at a distance z from the wall (or from the midpoint between the walls in the case of AS capillary bridges; see Figure 1g), we calculate the average density $\rho_{slab}(r)$ as a function of the distance r from the z-axis. Specifically, we divide the slab into thin rings of inner and outer radii r and $r + \Delta r$, respectively, where Δr = 0.5 Å, and calculate the average number of water O atoms in the ring. As expected, $\rho_{slab}(r)$ is constant within the droplet/bridge, and it decays abruptly to practically zero in the vapor phase. Hence, we define the droplet/bridge radius at height z, $r_{prof}(z)$, as the distance r at which $\rho_{slab}(r) = \rho_0 = 0.2$ g/cm^3 (our results are not sensitive to slight variations in ρ_0). The function $r_{prof}(z)$ provides the droplet/bridge profile for the given snapshot. By averaging $r_{prof}(z)$ over the 2000 snapshots, we obtain the final droplet/bridge profile.

A similar procedure is employed to calculate the profiles of TS droplets and TS bridges (Figure 1f,h). As before, for each snapshot, we identify the droplet/bridge center of mass and define a z-axis passing through it, perpendicular to the wall(s). The droplet/bridge is divided into slabs, as explained previously and for each slab, centered at a distance z from the wall (or from the midpoint between the walls in the case of TS capillary bridges; see Figure 1h), we calculate the average density $\rho_{slab}(r)$. However, for TS droplets/bridges, we divide the slab into rods parallel to the y-axis, with inner and outer coordinates r and $r + \Delta r$, respectively, where Δr = 0.5 Å (note that in these cases r is defined as the distance to the x = 0 plane). The distance r at which $\rho_{slab}(r) = \rho_0 = 0.2$ g/cm^3 defines the boundary of the droplet/bridge. By averaging $r_{prof}(z)$ over the last 2000 snapshots of the simulation, we obtain the final droplet/bridge profile.

In the case of AS and TS bridges, the liquid bridge must be symmetric with respect to its middle-height point (i.e., the bridge neck) which is located at the midpoint between the walls, z = 0 (Figure 1g,h). Accordingly, for bridge profile calculations, we take the average of $r_{prof}(z)$ and $r_{prof}(-z)$ and report the profile only for $0 \le z \le h/2$.

2. Droplet and Bridge Profiles from Capillarity Theory. Based on the concept of surface tension, CT predicts that the density profiles of AS droplets on a surface are spherical

$$r(z)^2 + (z - z_c)^2 = R^2 \quad (1)$$

where $r(z)$ is the radius of the droplet at height z and R is the radius of the droplet profile (see Figure 1e). The spherical

DOI: 10.1021/acs.jpcc.5b10377
J. Phys. Chem. C 2016, 120, 1597−1608

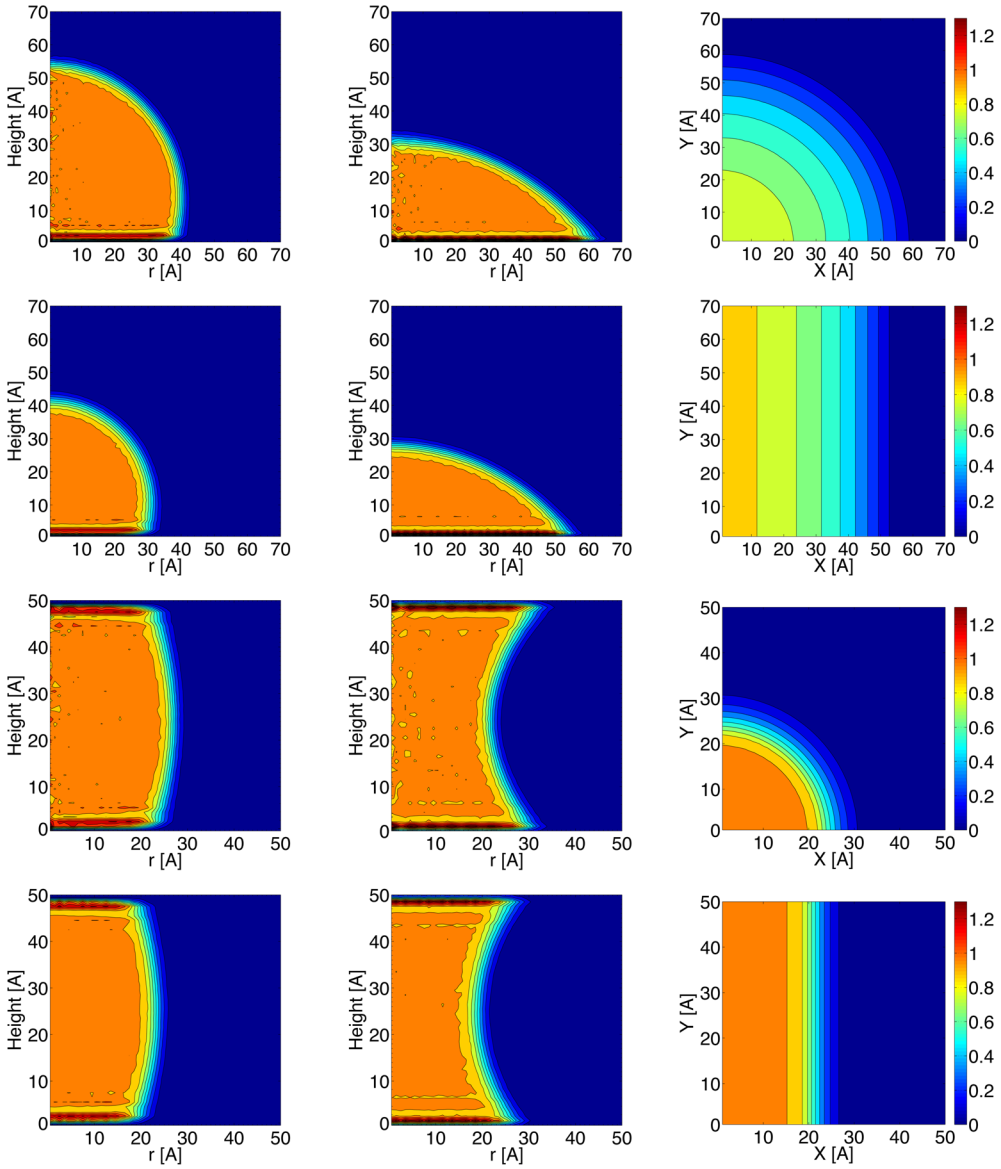

Figure 2. Density contour maps for the droplets and bridges in contact with hydrophobic (k = 0.0, left column) and hydrophilic (k = 0.6, middle column) surfaces. The right column shows the top view of the droplet/bridges in contact with the hydrophilic (k = 0.6) surface. The first and second row are the density contour maps of the large AS and TS droplets, respectively; the density contour maps of AS and TS bridges are shown in the third and fourth row, respectively. Color bars indicate the density scale in g/cm^3 [for comparison, we note that the density of bulk SPC/E water at the present temperature (T = 300 K) and P = 0.1 MPa is ≈1 g/cm^3 [41]].

profile is centered on the z-axis, at height z_c, and the wall is located at z = 0. Equation 1 is also valid for TS droplets provided that $r(z)$ is defined as half the thickness of the droplet at height z (Figure 1f).

In the case of AS bridges, the expression for $r(z)$ is not trivial and involves special functions (see, e.g., ref 39). In this case, the following differential equation can be used to define the density profile (see Appendix)

$$\left|\frac{dz}{dr}\right| = \frac{|H(r^2 - r_0^2) + r_0|}{\sqrt{r^2 - [H(r^2 - r_0^2) + r_0]^2}} \quad (2)$$

where $r(z)$ is the radius of the AS bridge at height z, $H = (1/R_1 + 1/R_2)/2$ is the average surface curvature of the bridge,[1] R_1 and R_2 are the surface radii of curvature, and r_0 is the bridge radius at z = 0, i.e., at half the bridge's height (Figure 1g). We follow the sign convention of ref 1, where R_1 and R_2 can be positive or negative. For given values of H and r_0, eq 2 can be integrated numerically and the bridge profile $r(z)$ can be calculated.

For TS bridges, the average surface curvature is $H = 1/(2R_2)$, i.e., $R_1 = \infty$ (compare Figures 1g and 1h). Since the average surface curvature of the TS bridge is constant, it follows that the TS bridge profile is a circle of radius R_2. The circular profile is centered at z_c = 0 and $r_c = r_0 - R_2$, where r_0 is half the *thickness* of the bridge at z = 0, i.e.,

$$[r(z) - r_c]^2 + z^2 = {R_2}^2 \quad (3)$$

The theoretical profiles $r(z)$ resulting from eqs 1−3 are used to fit the droplets/bridge profiles obtained from MD simulations. The theoretical profiles only require the parameters (R, z_c) for the case of AS and TS droplets and (H, r_0) for the case of AS and TS bridges. In order to identify the parameters that best fit the simulation profiles, we use the

DOI: 10.1021/acs.jpcc.5b10377
J. Phys. Chem. C 2016, 120, 1597−1608

following procedure. (i) On the basis of the MD simulations droplet/bridge profile, we define a reasonable range for the fitting parameters (R, z_c), for the case of droplets, and (H, r_0), for the case of bridges. We set these parameters to the corresponding lowest values to be explored and calculate the theoretical profiles $r(z)$ using eq 1, 2, or 3. (ii) For each point i of the droplet/bridge profile, (r_i, z_i), obtained from the MD simulation, we calculate the corresponding distance d_i to the theoretical profile $r(z)$. Specifically, from each point (r_i, z_i) we find a line which crosses the curve $r(z)$ at a right angle and measure the distance between the crossing point and point (r_i, z_i). (iii) We calculate the error between the theoretical and MD simulation profile as

$$\epsilon = \sqrt{\frac{1}{N_p}\sum_{i=1}^{N_p} d_i^2} \tag{4}$$

where N_p is the number of points of the droplet/bridge profile obtained from the MD simulation. (iv) We change the parameters (R, z_c) (droplets) or (H, r_0) (bridges) by small increments and repeat steps ii−iv until the whole range of the parameters is covered.

For each set of values (R, z_c) or (H, r_0) we obtain a value of ϵ. The set of parameters for which ϵ is minimum provides together with eqs 1−3, the theoretical droplet/bridge profiles.

We note that knowledge of the parameters (R, z_c) or (H, r_0) allows one to calculate any geometrical property of the droplets and bridges. For example, the contact angles for the AS and TS droplets can be obtained from the (R, z_c) parameters using eq 21 of the Appendix. Similarly, the contact angle between a TS bridge and the wall can be calculated using eq 3, and it is given by

$$\theta_c = 90^\circ + \frac{180^\circ}{\pi}\arcsin(hH) \tag{5}$$

The contact angle for the AS bridges is obtained from the derivative of the profile given by eq 2 evaluated at $z = \pm h/2$, i.e., at one of the surfaces.

3. Density Contour Maps. The density contour maps (DCMs) provide complementary information to the droplets/bridges profiles. To obtain the DCM, we divide the system box into cells of dimensions $1 \times 1 \times 1$ Å^3. For each cell i centered at location (x_i, y_i, z_i), we calculate the average local density $\rho(x_i,y_i,z_i)$. As for the density profile, $\rho(x_i,y_i,z_i)$ is calculated by averaging over the last 2 ns of the simulation.

For AS droplets and AS bridges, we average the density field $\rho(x_i,y_i,z_i)$ over boxes in the $z = z_i$ plane, intersected by cylinders of radii r_i, and generate a *radial* density map $\rho(r_i,z_i)$. Specifically, $\rho(r_i,z_i)$ is the density averaged over boxes with coordinates (x_j, y_j, z_j) that satisfy $r_i = (x_j^2 + y_j^2)^{1/2}$ and $z_j = z_i$. The set of values $\rho(r_i,z_i)$ are used to construct the *side view* of the DCM, $\rho_{side}(r,z)$. The first and third rows of Figure 2, columns one and two, show $\rho_{side}(r,z)$ for AS droplets and AS bridges.

In the case of TS droplets and TS bridges, the *side view* of the DCM $\rho_{side}(r,z)$ is constructed by averaging $\rho(x_i,y_i,z_i)$ over all boxes in the $z = z_i$ plane and intersected by vertical *planes* perpendicular to the x-axis (the TS droplets and TS bridges are periodic along the y-axis). Specifically, $\rho(r_i,z_i)$ is the density averaged over boxes with coordinates (x_j, y_j, z_j) that satisfy $|x_j| = r_i$ and $z_j = z_i$. The second and fourth rows of Figure 2, columns one and two, show $\rho_{side}(r,z)$ for TS droplets and TS bridges.

For all droplets and bridges, we also calculate the projection of the density field $\rho(x_i,y_i,z_i)$ on the xy-plane. This provides a *top* view of the density map, $\rho_{top}(x,y)$; see, e.g., third column of Figure 2. This is done by averaging the density field $\rho(x_i,y_i,z_i)$ over all z_i values, for fixed x_i and y_i. We note that the density map $\rho_{top}(x,y)$ is sensitive on the range of values of z_i used to average $\rho(x_i,y_i,z_i)$. In the case of capillary bridges, this range is clearly the bridge height, h = 50 Å. In the case of droplets, we use the height of the drop at z = 0, as defined from the corresponding $\rho_{side}(r,z)$.

III. RESULTS

A. Droplets and Bridges Profiles and Density Contour Maps. Figure 2 shows the density maps for different geometries and two values of the surface polarity k. The first and second columns show the side view of the DCM of (top to bottom) AS droplets, TS droplets, AS bridges, and TS bridges for k = 0.0 and k = 0.6, respectively. The third column shows the top view of the DCM for the same geometries and for k = 0.6. Two main observations follow from Figure 2. (i) In all cases, the liquid−vapor interface is rather sharp, 5−10 Å thick, and the density of water decreases monotonically as the vapor phase is approached. Instead, water at the solid interface is rather structured with nonmonotonic density changes along the z-direction (perpendicular to the wall), which is consistent with previous studies.[38,40] (ii) The density of *bulk* SPC/E water is ≈1 g/cm^3 at $P \approx 0$ and T = 300 K.[41] Interestingly, all DCMs in Figure 2 exhibit regions where the density is ≈1 g/cm^3, suggesting that all bridges/droplets have a domain of bulk-like water. That this should be the case is not evident given the small dimensions of some of the geometries studied, 2−3 nm, and the presence of interface fluctuations inherent to liquid−vapor interfaces.

Next, we compare the density profiles obtained from MD simulations and the corresponding predictions from CT (eqs 1−3). The profiles for AS and TS droplets are shown in Figures 3a and 3b while the profiles for AS and TS bridges are shown in Figures 4a and 4b. The agreement between CT and MD simulations is remarkable, for all droplets/bridges and surface hydrophobicity/hydrophilicity. The fitting parameters of the density profiles in Figures 3 and 4, for all geometries and values of k, are presented in Tables 1 and 2.

One of the most important assumptions of (macroscopic) CT is that the contact angle of a liquid is independent of the geometry of the interfaces involved. To test this point, we include in Tables 1 and 2 the contact angles θ_c of the water droplets and bridges studied, for all values of k; the corresponding values of θ_c as a function of k are shown in Figure 5a. Our MD simulations indicate that indeed water contact angle is independent of the geometry of the interfaces involved and it depends solely on the walls considered (i.e., $\theta_c = \theta_c(k)$). Similar findings have been reported for nanodroplets sitting above hydrophilic patches of heterogeneous surfaces.[32] In particular, since water contact angle depends on the liquid−liquid, liquid−solid, and liquid−vapor surface tensions, the present results also suggest that at 2−10 nm scales the surface tensions can be treated as independent of the interfaces' curvature, a rather nontrivial result (see, e.g., ref 42).

We also stress that in the comparison of the density profiles from theory and simulations we did not include any *line* tension. Indeed, our results indicate that for >2 nm scales droplets/bridges the line tension plays a minor role. To show this, we focus on the values of θ_c obtained from the small AS, large AS, and TS droplets (Table 1). The correction in the calculated values of $\theta_c(k)$ due to a nonzero line tension $\tau(k)$

DOI: 10.1021/acs.jpcc.5b10377
J. Phys. Chem. C 2016, 120, 1597−1608

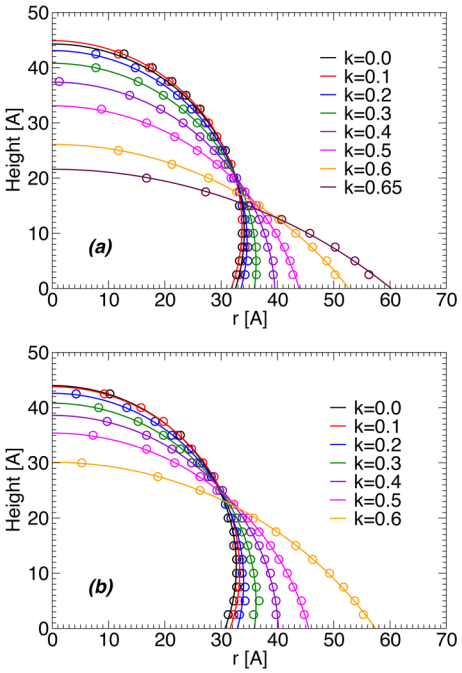

Figure 3. Profiles of (a) small AS and (b) TS droplets in contact with surfaces of different surface polarities, k, from MD simulations (circles). r in (a) is the AS-droplet *radius*; r in (b) is half the TS-droplet *thickness*. Lines are the best fits obtained using eq 1, predicted by CT. In (a) and (b), the simulation box side length is L = 138.6 Å, and only one-half of the droplet is shown. The theoretical profiles from CT fit remarkably well the drop profiles of the AS and TS droplets even for the ≈20 Å height droplet in (a), i.e., at dimensions where the concept of surface tension is not evident. Small (N = 3375, L = 138.6 Å) and large (N = 6750, L = 277.2 Å) AS droplets wet the surface for $k \geq 0.7$. The TS droplets in (b) wet the surface for $k \geq 0.65$, instead of $k \geq 0.7$, due to periodic boundary conditions and large number of molecules composing the droplet (N = 9897, L = 138.6 Å).

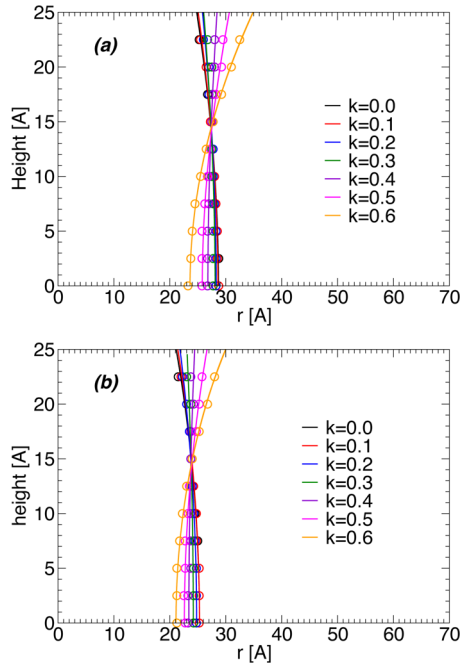

Figure 4. Profiles of (a) AS and (b) TS bridges in contact with surfaces of different surface polarities, k, from MD simulations (circles). r in (a) is the AS-bridge *radius*; r in (b) is half the TS-bridge *thickness*. Lines are the best fits obtained using eqs 2 and 3, predicted by CT. In (a) and (b), the walls are separated by 50 Å, and only the upper half of the bridge is shown. The theoretical profiles from CT fit remarkably well the profile of the AS and TS bridges even for bridges with minimum radius/half thickness (at zero height) of ≈20 Å, i.e., at dimensions where the concept of surface tension is not evident. AS (N = 3375, L = 138.6 Å) and TS bridges (N = 9897, L = 138.6 Å) wet the surface for $k \geq 0.7$.

can be obtained from the modified Young equation,[19,43] and it is given by $\cos\theta_c(r_B) - \cos\theta_\infty = -\tau/(\gamma_{LV} + r_B)$, where γ_{LV} is the liquid–vapor surface tension, r_B is the radius of the droplet base (Figure 1e,f), and θ_∞ is the macroscopic contact angle given by Young's equation, $\cos\theta_\infty = (\gamma_{SV} - \gamma_{SL})/\gamma_{LV}$. Thus, the contact angle obtained from the TS droplet is the true, i.e., macroscopic, water contact angle ($r_B = \infty$). In particular, a nonzero $\tau(k)$ implies that the values of $\theta_c(k)$ should differ among the small AS, large AS, and TS droplets. However, a comparison of the values of θ_c given in Table 1 indicates that $|\Delta\theta_c(k)| \leq 3.5°$. This is close to the difference in θ_c between the small and large AS droplets (Table 1). Therefore, any effect of τ in the studied systems is within the error bars in the calculated θ_c. Negligible line tensions have been also found in the case of water droplets in contact with amorphous silica surfaces.[44]

It follows from this discussion that the concept of contact angle and surface tension hold even at the 2–10 nm scale, which is surprising given the small length scales of the systems considered. For example, the smallest droplet studied in contact with the k = 0.65 surface is only 2 nm high while the thickness of the liquid–vapor interface is 0.8–1 nm and the typical thickness of the solid–water interface is ≈1–1.4 nm.[40] Hence, there is very little space left within this droplet to contain bulk-like water.

The functional form of $\cos\theta_c(k)$ [Figure 5b] can be fitted very well by a quadratic polynomial $\cos\theta_c(k) = -0.31 - 0.18k + 2.82k^2$. Such a quadratic dependence on k can be rationalized in terms of the Young equation which states that $\cos\theta_c = (\gamma_{SG} - \gamma_{LS})/\gamma_{LG}$, where γ_{SG}, γ_{LS}, and γ_{LG} are the solid–gas, liquid–solid, and liquid–gas surface tensions. We can assume that γ_{LG} is independent of k while γ_{SG} should depend only weakly on k due to the low density of the vapor. The dominant dependence on k is thus given by the liquid–solid interface energy. This surface energy should behave as $\gamma_{LS}(k) = a - bk^2$, where a and b are some constants. This is because the main contribution to the solid–liquid energy is the dipole–dipole interactions between the water molecules and the surface silanol groups. Since the surface dipole moment causes polarization of the water layer next to the interface (see ref 37), which is proportional to k, then the interaction energy of the surface and the water layer at the interface should be proportional to $-k^2$. A similar argument is presented in ref 1. However, the argument in ref 1 is based on the concept of polarizability which occurs due to van der Waals interactions. In our MD simulations, polarizabilities are omitted. Accordingly, the dependence of $\cos\theta_c$ on k in our model system is different from the corresponding expression presented in page ref 1.

B. Force, Pressure and Surface Tension for Water AS and TS Bridges. In this section, we focus on AS and TS bridges and study the forces and pressures that the water bridges exert on walls with different surface polarities, k. This is important for practical applications, e.g., to quantify forces

DOI: 10.1021/acs.jpcc.5b10377
J. Phys. Chem. C 2016, 120, 1597–1608

Table 1. Fitting Parameters for the AS and TS Droplet Profiles (see Figure 1e,f)[a] Using Eq 1

	small AS droplets				large AS droplets				TS droplets			
k	R	z_c	θ_c	ϵ	R	z_c	θ_c	ϵ	R (Å)	z_c (Å)	$\theta_{c\,(deg)}$ (deg)	ϵ (Å)
0.0	33.7	11.2	109.4	0.15	42.0	14.0	109.5	0.18	32.7	11.3	110.2	0.15
0.1	34.1	10.2	107.4	0.21	42.6	12.5	107.0	0.15	33.3	10.5	108.4	0.18
0.2	34.6	8.5	104.2	0.21	43.4	10.4	103.9	0.21	34.0	8.6	104.7	0.19
0.3	36.2	4.6	97.3	0.10	45.0	6.2	97.9	0.18	36.2	4.6	97.3	0.20
0.4	39.6	−2.2	86.8	0.15	48.8	−1.7	88.0	0.19	40.2	−1.6	87.7	0.12
0.5	45.6	−12.5	74.1	0.15	57.4	−16.2	77.6	0.18	47.0	−11.6	75.7	0.13
0.6	66.2	−40.1	52.7	0.14	78.8	−45.4	54.8	0.16	69.8	−39.7	55.3	0.15
0.65	94.7	−73.1	39.5	0.21	121.9	−95.7	38.3	0.12				

[a] ϵ is the error in of the fitting curve from eq 4. Errors in R and z_c are ±0.05 Å. TS droplets wet the surface for $k \geq 0.65$.

Table 2. Fitting Parameters for the AS and TS Bridge Profiles see Figure 1g,h) Using Eqs 2 and 3[a]

	AS bridges					TS bridges				
k	R_1 (Å)	R_2 (Å)	H (Å^{-1})	θ_2 (deg)	ϵ (Å)	r_0 (Å)	R_2 (Å)	H (Å^{-1})	θ_c (deg)	ϵ (Å)
0.0	28.8	80.4	0.0236	106.6	0.18	25.3	77.1	0.0065	108.9	0.20
0.1	28.7	84.4	0.0233	105.7	0.14	25.3	82.5	0.0061	107.6	0.12
0.2	28.2	126.6	0.0217	100.3	0.12	24.8	106.4	0.0047	103.6	0.08
0.3	27.8	225.9	0.0202	95.7	0.09	24.2	290.0	0.0017	94.9	0.18
0.4	26.8	−229.0	0.0165	84.6	0.18	23.4	−300.0	−0.0017	85.2	0.24
0.5	25.7	−60.0	0.0111	70.0	0.15	22.6	−79.2	−0.0063	71.6	0.12
0.6	23.8	−29.8	0.0042	50.11	0.12	21.1	−39.6	−0.0126	50.9	0.12
0.65	22.2	−21.9	−0.0003	34.75	0.16					

[a] R_1 and R_2 are the radii of curvature of the bridge neck (i.e., at its middle-height point) on the x−y-plane and x−z-plane, respectively (see Figure 1g,h). $H = (1/2)(1/R_1 + 1/R_2)$ is the average surface curvature of the bridge, θ_c is the contact angle, and ϵ is the error of the fitting curve from eq 4. For TS bridges, $R_1 = \infty$; r_0 is the thickness of the bridge neck. Errors in r_0, R_1, and R_2 are ±0.05 Å.

induced by capillary bridges in AFM experiments and in granular materials where humidity can induce the formation of capillary bridges between surfaces. Yet, the main motivation of this section is to perform another test of CT at the 2−10 nm scale. Specifically, the forces and pressures on the surfaces induced by the bridges can be calculated directly from our MD simulations for different values of k (or contact angles θ_c), and these quantities can be compared with the corresponding predictions from CT.

During the MD simulations, we measure the force produced by the AS and TS bridges on each wall by calculating the sum of the forces between all water molecules and all atoms in the given wall. We evaluate the components F_x, F_y, and F_z of the total force averaged over time. For both AS and TS droplets, the time averages of F_x and F_y converge to zero for large times, as expected, and hence, their deviations from zero provide an estimation of the force error bars. In addition, due to the symmetry of the system, we average the normal components of the force acting on the two walls: $F_z = (\vec{F}_1 \cdot \check{n}_1 + \vec{F}_2 \cdot \check{n}_2)/2$, where $\vec{F}_i$ is the force acting on wall i = 1, 2 and $\check{n}_i$ is a unit vector perpendicular to wall i, pointing toward the bridge. We note that from the calculated F_z we are able to measure other properties, such as the surface tension of water and the pressure inside the water bridges.

The net force along the z-axis at *any* cross section of the bridge must be constant,[1] independently of whether the bridge is AS or TS. Hence, if $F_{z,\mathrm{neck}}$ is the force acting on a plane perpendicular to the bridge and passing through the capillary bridge's neck (i.e., at $z = 0$), it must be that $F_{z,\mathrm{neck}} = F_z$. It can be shown that[1]

$$F_z = F_\gamma + F_P \tag{6}$$

where F_γ is the force on the wall due the liquid−vapor surface tension γ and $F_P = PA_b$ is the force on the wall due to the pressure P within the water bridge; here, A_b is the area of the bridge's base. For AS bridges, $F_\gamma = 2\pi\gamma r_b \sin\theta_c$ and $F_P = P(\pi r_b^2)$ (Figure 1g). For the TS bridges, $F_\gamma = 2L\gamma \sin\theta_c$ and $F_P = P(2Lr_b)$, where L is the bridge's length (equal to the box side length) and r_b is *half* the thickness of the bridge's base (see Figure 1h). Using Young−Laplace equation and assuming $P \approx 0$ in the vapor phase, one can write $P = -2\gamma H$. Therefore, the forces produced by the bridges on the walls are

$$F_z = 2\pi r_b \gamma \sin\theta_c - 2\pi r_b^2 \gamma H \tag{7}$$

for AS bridges and

$$F_z = 2L\gamma \sin\theta_c - 4Lr_b\gamma H \tag{8}$$

for TS bridges.

Similarly, the force at the neck of the AS bridge is given by

$$F_{z,\mathrm{neck}} = 2\pi r_0 \gamma - 2\pi r_0^2 \gamma H = 2\pi\gamma C \tag{9}$$

where $C = r_0 - Hr_0^2$. For TS bridges, we obtain

$$F_{z,\mathrm{neck}} = 2L\gamma - 4Lr_b\gamma H = 2\gamma C \tag{10}$$

where $C = L - 2Lr_bH$. C is the neck parameter and can be obtained from Table 2. We note that since we are considering different surface polarities, $C = C(k)$.

The condition $F_{z,\mathrm{neck}} = F_z$ together with eqs 9 and 10 provide strong tests of CT for the MD simulations of the AS and TS bridges. Specifically, CT predicts that for AS bridges the force F_z from MD simulations must be a linear function of $C(k)$ and that the slope of this line should be $2\pi\gamma$. Similarly, for TS bridges, the force F_z must be a linear function of $C(k)$ with slope 2γ. Figure 6 shows that our MD simulations are fully

DOI: 10.1021/acs.jpcc.5b10377
J. Phys. Chem. C 2016, 120, 1597−1608

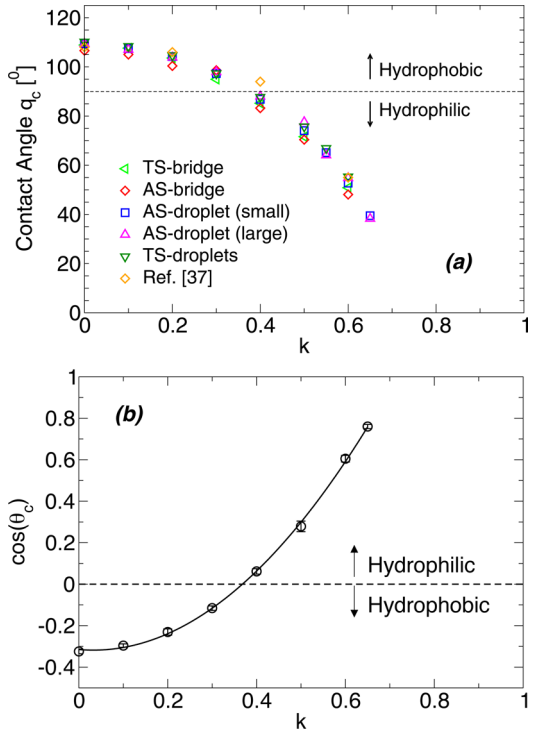

Figure 5. (a) Contact angles as a function of the surface polarity k obtained from the profiles in Figures 3a,b and 4a,b. For comparison, we also include the contact angles from the large droplet profiles (not shown) (N = 6750, L = 277.2 Å). Simulations for AS and TS droplets and bridges provide similar contact angles for all the walls considered. (b) Cosine of the average contact angle obtained from (a) as a function of k. The solid line is a quadratic fit. Dashed lines indicate θ_c = 90°. Surfaces for which θ_c > 90° (θ_c < 90°) are hydrophobic (hydrophilic).

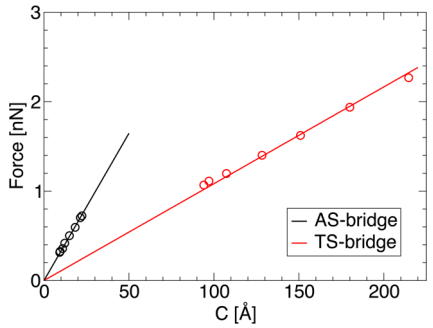

Figure 6. Force between walls induced by AS bridges and TS bridges as a function of the neck parameter C. $C = r_0 - Hr_0^2$ for AS bridges and $C = L - 2LHr_b$ for TS bridges (see text); values of C are obtained from Table 2. Lines are the best linear regression intercepting the origin. Error bars are smaller than the symbol size.

consistent with these predictions. Remarkably, the linear fits in Figure 6 (with zero intercept) for AS and TS bridges give, in both cases, γ = 0.054 ± 0.001 N/m^2. This value of γ is consistent with the values of the liquid–vapor surface tension of SPC/E water available in the literature[45,46] (see also next section).

We also test that the forces on the walls obtained from MD simulations obey eqs 7 and 8 for the case γ = 0.054 N/m^2. Figures 7a and 7b show, for both AS and TS bridges, the forces acting on the walls measured directly from the MD simulations and the corresponding values from eqs 7 and 8 (in these cases,

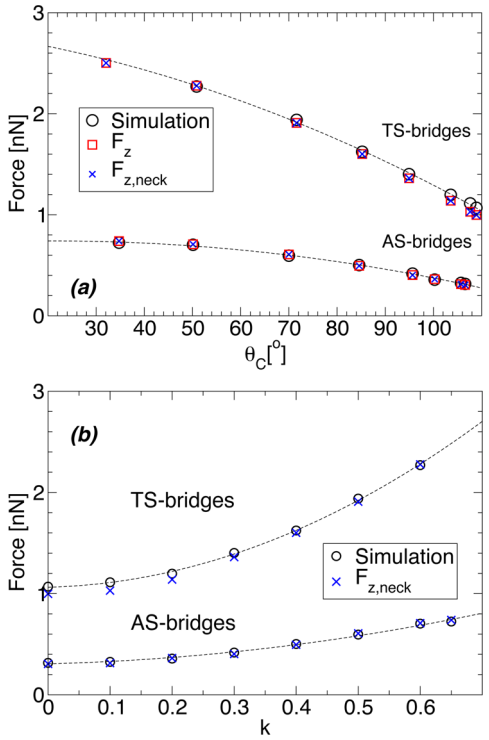

Figure 7. Forces induced by AS bridges and TS bridges formed between parallel walls as a function of (a) water contact angle and (b) normalized surface dipole moment k. F_z is the force that the water bridge exerts on the walls; black circles are results from MD simulations, and red squares are the predictions from CT. $F_{z,neck}$ (blue crosses) is the force at the bridge neck predicted by CT (see text). Error bars are smaller than the symbol size. Lines are quadratic polynomial fittings. For TS bridges in contact with surfaces with polarity k = 0.65, we observe large fluctuations of the liquid–vapor interface next to the walls leading to large errors in θ_c. Accordingly, the corresponding value of the force is omitted in (a) and (b).

the values of r_b are obtained from the bridge profiles in Figure 4). Again, the agreement between MD simulations and CT is excellent.

We also calculate the hydrostatic pressure that the water bridge exerts on the walls as a function of the contact angle θ_c and surface polarity k. From eq 6, it follows that the pressure in the water bridge is given by

$$P = \frac{F_\gamma - F_z}{A_b} \tag{11}$$

which can be rewritten as

$$P = \frac{2\pi\gamma r_b \sin\theta_c - F_z}{\pi r_b^2} \tag{12}$$

for the case of AS bridges and

$$P = \frac{2L\gamma \sin\theta_c - F_z}{2r_b L} \tag{13}$$

for the case of TS bridges. We use these expressions to compute the pressures within AS and TS bridges from MD simulations (i.e., with γ = 0.054 N/m^2, r_b obtained from Figure 4, and F_z obtained from MD simulations). The theoretical value for the pressure is obtained from Young–Laplace equation, eq 14, considering that the pressure outside the water bridge is equal to zero and using the corresponding value of H from

DOI: 10.1021/acs.jpcc.5b10377
J. Phys. Chem. C 2016, 120, 1597–1608

Table 2. We verify that eqs 12 and 13 yield the same value of pressure predicted by eq 14; the corresponding values of P as a function of k and θ_c are shown in Figures 8a and 8b.

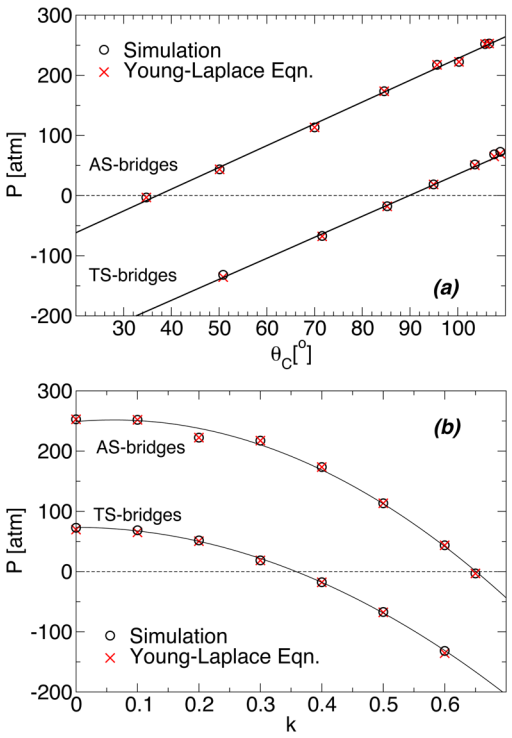

Figure 8. Pressure inside the AS and TS bridges as a function of (a) water contact angle and (b) normalized surface dipole moment k. Red crosses are the pressures from CT derived using Young−Laplace equation; circles are the pressures obtained from the forces acting on the walls calculated from the MD simulations. Solid lines in (a) are linear interpolations; solid lines in (b) are quadratic polynomials fittings. For hydrophilic surfaces, pressures become negative (i.e., water is under tension) for $\theta_c < 37°$ and $\theta_c < 90°$ in the case of AS bridges and TS bridges, respectively. For hydrophobic surfaces, pressures become very large; e.g., for $\theta_c \approx 106°$ ($k = 1$), $P \approx 250$ and 70 atm for AS bridges and TS bridges, respectively.

A surprising result follows from Figure 8a. The results from MD simulations indicate that for $\theta_c < 37°$ and $\theta_c < 90°$, for the case of AS and TS bridges, respectively, the pressure on the walls is negative. Therefore, nanoscale bridges in the 2−10 nm range formed between hydrophilic surfaces may contain water under tension. This is consistent with recent experiments of nanoscale water bridges were the internal water pressure was estimated to be −160 MPa.[47−49] We stress that the pressure inside macroscopic AS bridges is always positive, and hence, this is a phenomenon inherent to the nanoscale dimensions explored. We also note the pressure inside the bridges can be very large (Figure 8a), ≈250 atm, which is 2 orders of magnitude larger than the pressure of water bridges of ≈1 μm in size. It follows from this discussion that similar conclusions may hold for the *forces* that the water bridges exerts on the walls. For example, Figure 7 suggests that for large θ_c one may find that $F_z < 0$.

C. Calculating the Surface Tension with Kirkwood−Buff (KB) Method. We used the Kirkwood−Buff (KB) method[50] to test the self-consistency of CT at the nanometer scale. In this method, an orthorhombic simulation box ($L_x = L_y < L_z$) is created, and a slab of water molecules is placed at the middle of the box, parallel to the xy-plane, with a vacuum space above and below the water slab. Hence, the two liquid−vapor interfaces exist during the MD simulation. The surface tension γ can be calculated using the expression $\gamma = L_z\langle 2P_{zz} - P_{xx} - P_{yy}\rangle/4$, where P_{xx}, P_{yy}, and P_{zz} are the diagonal components of the stress tensor. To calculate γ using the KB method, we simulate a water slab of $N = 3375$ water molecules in an orthorhombic box with dimensions $L_x = L_y = 50$ Å and $L_z = 140$ Å. The simulation is run for 5 ns using the LAMMPS package and the principal component of the pressure tensor are calculated. At $T = 300$ K, we obtain $\langle P_{zz}\rangle = -2.8 \pm 1.3$ atm, $\langle P_{yy}\rangle = -81.7 \pm 1.7$ atm, and $\langle P_{xx}\rangle = -81.9 \pm 1.4$ atm, resulting in a value of $\gamma = 0.056 \pm 0.001$ N/m^2. This value is in good agreement with the value obtained from the studies of the nanoscale AS and TS bridge as well as with the values known from the literature for SPC/E water.[50]

IV. SUMMARY AND DISCUSSION

In summary, we present results from MD simulations of water droplets and bridges in contact with a family of hydrophobic/hydrophilic surfaces characterized by different surface polarities. Our study is based on four different geometries: AS droplets, TS droplets, AS bridges, and TS bridges. From the MD simulations, we calculate the profile of the different droplets/bridges and compare them with the corresponding prediction of macroscopic CT. We find an excellent agreement between the theory and simulations, even when the droplets/bridges studied are very small, with dimensions as small as 2 nm. We also calculate the contact angle of the droplets/bridges in contact with different walls and confirm that as assumed by CT, these contact angles are independent of the droplets/bridges geometry and depend solely on the walls considered.

In order to test the self-consistency of CT at 2−10 nm scales, we also calculate the capillary forces of AS and TS bridges formed between parallel walls. These forces are calculated directly from MD simulations and compared with the corresponding expressions of CT. Again, we find an excellent agreement between theory and simulations. We note that the physical quantities involved in these expressions are consistent with independent calculations. For example, the expressions for the forces produced by the bridges on the walls are correct if the liquid−vapor tension of SPC/E water is $\gamma \approx 0.054$ N/m^2. This value is in good agreement with the value of γ obtained using the Kirkwood−Buff method for a flat interface, and it is also consistent with the values of γ for SPC/E water reported in the literature.[50]

Our MD simulations clearly demonstrate that the predictions of the macroscopic CT are correct at the nanoscale when the dimensions of the droplets/bridges are only several nanometers. This makes an important statement that CT can be successfully used to e.g. interpret results of the AFM experiments. We note that our simulations indicate that in order to describe the behavior of 2−10 nm size droplets and bridges, the surface tensions can be assumed to be independent of the droplets/bridges size and, hence, of the large surface curvature of these interfaces. In addition, we find no need to include line tensions to describe the geometries of the droplets/bridges studied, i.e., at 2−10 nm scales.

Another important conclusion is that straightforward MD simulations of a scaled down model can successfully describe the capillarity phenomena in the system of the same geometry at micron and millimeter scales. These macroscopic phenomena can be simulated by various analytical and finite element

DOI: 10.1021/acs.jpcc.5b10377
J. Phys. Chem. C 2016, 120, 1597−1608

methods. However, these methods are not easy to implement for a particular geometry, and hence MD simulations can provide a useful consistency check in these complex situations.

Beside these practical problems, our simulations suggests that CT may be applicable to fundamental problems involving the emergence of surface tension at the nanoscales where the characteristic lengths of the interface density fluctuations are comparable to the system size, such as in the case of homogeneous/heterogeneous nucleation and critical phenomena,[51−54] capillary condensation in nanoscale confinement, and dynamics of contact line spreading.[55,56]

APPENDIX. DROPLET/BRIDGE PROFILES FROM MACROSCOPIC CAPILLARITY THEORY

In this section, we outline a derivation for the expressions from CT that describe the profiles of AS and TS droplets as well as AS bridges (eqs 1 and 2); the corresponding expression from CT for the case of TS bridges (eq 3) is trivial (see section II.B.2).

There are two fundamental expressions in classical CT: the Young−Laplace equation and the Young equation. The Young−Laplace equation relates the difference in pressure across an interface, $\Delta P = P_{in} - P_{out}$ where P_{in} and P_{out} are the pressures on both sides of the interface. Specifically, it states that

$$\Delta P = \gamma_{LG} 2H \quad \text{with } H = \frac{1}{2}\left(\frac{1}{R_1} + \frac{1}{R_2}\right) \tag{14}$$

Here, γ_{LG} is the surface tension of the interface (gas−liquid interface, in our case), H is the mean curvature of the interface, and R_1 and R_2 are the principal radii of curvature (R_1 and R_2 can be negative or positive; see ref 1). Since the pressure in a liquid or gas at equilibrium must be constant at any point, the average curvature H must be constant over the entire interface.

The Young equation relates the equilibrium surface tensions of the liquid−gas (LG), liquid−solid (LS), and solid−gas (SG) interfaces at the three phase line, and it is given by

$$\cos\theta_c = \frac{\gamma_{SG} - \gamma_{LS}}{\gamma_{LG}} \tag{15}$$

where θ_c is the contact angle and γ_{LG}, γ_{LS}, and γ_{SG} are the different surface tensions involved.

Next, we describe how to obtain analytically the liquid profile for AS droplets, TS droplets, and AS bridges.

Profiles for AS and TS Droplets. We consider an AS droplet as shown in Figure 1e where $r(z)$ is the droplet radius at height z. For the volume of the droplet above a given height z, the net force along the z-axis must be zero. Hence, the pressures inside and outside the droplet and the surface tension must satisfy

$$2\pi r\gamma \cos\theta + P_{out} r^2 \pi - P_{in}\pi r^2 = 0 \tag{16}$$

where $\gamma = \gamma_{LG}$ and θ is the angle formed between the line tangent to the drop profile at height z and the z-axis, i.e., $dr/dz = \tan\theta$. It can be shown[1] that

$$\cos\theta = \frac{1}{\sqrt{1 + \dot{r}^2}} \tag{17}$$

Then, eq 16 can be written as

$$\frac{2\gamma}{\sqrt{1 + \dot{r}^2}} = \Delta P r \tag{18}$$

or, equivalently, using eq 14

$$\left(\frac{dr}{dz}\right)^2 = \frac{1}{(Hr)^2} - 1 \tag{19}$$

Simple substitution shows that the solution of this equation is a sphere

$$r(z) = (R^2 - (z - z_c)^2)^{1/2} \tag{20}$$

where $R = 1/H$ and z_c is a constant (equal to the distance from the center of the sphere to the origin). Considering that $r(z)|_{z=0} \equiv r_0 = R\sin\theta_c$, where θ_c is the droplet contact angle, one gets $z_c = -R\cos\theta_c$. Equation 20 is the same as eq 1. From the parameters R and z_c we can obtain the contact angle θ_c of the droplet

$$\theta_c = 180° - \frac{180°}{\pi}\arccos\left(\frac{z_c}{R}\right) \tag{21}$$

A similar analysis shows that eq 20 holds for the case of TS droplets provided that $r(z)$ is half the thickness of the bridge at height z (see Figure 1f). In this case, eq 16 is replaced by

$$2L\gamma \cos\theta + P_{out} L 2r - P_{in} L 2r = 0 \tag{22}$$

which leads to an equation similar to eq 19 (with different coefficeints), and hence, it has eq 20 as solution.

Profile for AS Bridges. We consider an AS bridge as shown in Figure 1g. The origin of the system is at $z = 0$, i.e., at the bridge's neck; the bridge radius at its neck is r_0.

Consider the volume of the AS bridge between two transverse sections at heights $z = 0$ and z. Since the bridge is not displacing with time, the net force acting on such a volume of the bridge must add to zero. Again, the main forces acting on this volume are due to the surface tension and the pressures inside and outside the bridge. Therefore, it must be that

$$-\gamma 2\pi r_0 + \gamma 2\pi r \cos\theta + (\pi r_0^2)P_{in} - (\pi r^2)P_{in} + [\pi(r^2 - r_0^2)]P_{out} = 0 \tag{23}$$

Using eqs 14 and 17, eq 23 implies that

$$\frac{dz}{dr} = \pm\frac{|H(r^2 - r_0^2) + r_0|}{\sqrt{r^2 - [H(r^2 - r_0^2) + r_0]^2}} \tag{24}$$

which is eq 2 that describe the profile of the AS bridge between hydrophilic (sign +) and hydrophobic (sign −) surfaces.

AUTHOR INFORMATION

Corresponding Author

*E-mail ngiovambattista@brooklyn.cuny.edu (N.G.).

Notes

The authors declare no competing financial interest.

ACKNOWLEDGMENTS

We thank Guillaume Stirnemann and Pablo G. Debenedetti for their contributions in the early stages of this project and for enlightening discussions. Support for this project was provided by a PSC-CUNY Award, jointly funded by The Professional Staff Congress and The City University of New York. A.B.A. acknowledge the Coordenação de Aperfeiçoamento de Pessoal de Nível Superior (CAPES) for support. This research was supported, in part, by a grant of computer time from the City University of New York High Performance Computing Center under NSF Grants CNS-0855217, CNS-0958379, and ACI-

DOI: 10.1021/acs.jpcc.5b10377
J. Phys. Chem. C 2016, 120, 1597−1608

1126113. S.V.B. thanks the Dr. Bernard W. Gamson Computational Science Center at Yeshiva College for support.

REFERENCES

(1) de Gennes, P.; Brochard-Wyart, F.; Quéré, D. *Capillarity and Wetting Phenomena: Drops, Bubbles, Pearls, Waves*; Springer: 2004.
(2) Hornbaker, D. J.; Albert, R.; Albert, I.; Barabasi, A. L.; Schiffer, P. What Keeps Sandcastles Standing? *Nature* **1997**, *387*, 765−765.
(3) Hu, D. L.; Chan, B.; Bush, J. W. M. The Hydrodynamics of Water Strider Locomotion. *Nature* **2003**, *424*, 663−666.
(4) Eisner, T.; Aneshansley, D. J. Defense by Foot Adhesion in a Beetle (Hemisphaerota cyanea). *Proc. Natl. Acad. Sci. U. S. A.* **2000**, *97*, 6568−6573.
(5) Federle, W.; Riehle, M.; Curtis, A. S.; Full, R. J. An Integrative Study of Insect Adhesion: Mechanics and Wet Adhesion of Pretarsal Pads in Ants. *Integr. Comp. Biol.* **2002**, *42*, 1100−1106.
(6) Grotberg, J. B. Respiratory Fluid Mechanics. *Phys. Fluids* **2011**, *23*, 021301.
(7) Alencar, A. M.; Buldyrev, S. V.; Majumdar, A.; Stanley, H. E.; Suki, B. Avalanche Dynamics of Crackle Sound. *Phys. Rev. Lett.* **2001**, *87*, 088101.
(8) van Honschoten, J. W.; Brunets, N.; Tas, N. R. Capillarity at the Nanoscale. *Chem. Soc. Rev.* **2010**, *39*, 1096−1114.
(9) Bonn, D.; Eggers, J.; Indekeu, J.; Meunier, J.; Rolley, E. Wetting and Spreading. *Rev. Mod. Phys.* **2009**, *81*, 739−805.
(10) Weeks, B. L.; Vaughn, M. W.; DeYoreo, J. J. Direct Imaging of Meniscus Formation in Atomic Force Microscopy Using Environmental Scanning Electron Microscopy. *Langmuir* **2005**, *21*, 8096−8098.
(11) Schenk, M.; Füting, M.; Reichelt, R. Direct Visualization of the Dynamic Behavior of a Water Meniscus by Scanning Electron Microscopy. *J. Appl. Phys.* **1998**, *84*, 4880−4884.
(12) Sedin, D. L.; Rowlen, K. L. Adhesion Forces Measured by Atomic Force Microscopy in Humid Air. *Anal. Chem.* **2000**, *72*, 2183−2189.
(13) Yang, L.; Tu, Y.-s.; Tan, H.-l. Influence of Atomic Force Microscope (AFM) Probe Shape on Adhesion Force Measured in Humidity Environment. *Appl. Math. Mech., Engl. Ed.* **2014**, *35*, 567.
(14) Piner, R. D.; Zhu, J.; Xu, F.; Hong, S.; Mirkin, C. A. "Dip-Pen" Nanolithografy. *Science* **1999**, *283*, 661−663.
(15) Huppmann, W.; Riegger, H. Modelling of Rearrangement Processes in Liquid Phase Sintering. *Acta Metall.* **1975**, *23*, 965−971.
(16) Qian, B.; Breuer, K. S. The Motion, Stability and Breakup of a Stretching Liquid Bridge with a Receding Contact Line. *J. Fluid Mech.* **2011**, *666*, 554−572.
(17) Darhuber, A. A.; Troian, S. M.; Wagner, S. Physical Mechanisms Governing Pattern Fidelity in Microscale Offset Printing. *J. Appl. Phys.* **2001**, *90*, 3602−3609.
(18) Kang, H. W.; Sung, H. J.; Lee, T.-M.; Kim, D.-S.; Kim, C.-J. Liquid Transfer Between Two Separating Plates for Micro-Gravure-Offset Printing. *J. Micromech. Microeng.* **2009**, *19*, 015025.
(19) Werder, T.; Walther, J. H.; Jaffe, R. L.; Halicioglu, T.; Koumoutsakos, P. On the Water-Carbon Interaction for Use in Molecular Dynamics Simulations of Graphite and Carbon Nanotubes. *J. Phys. Chem. B* **2003**, *107*, 1345−1352.
(20) Koishi, T.; Yoo, S.; Yasuoka, K.; Zeng, X. C.; Narumi, T.; Susukita, R.; Kawai, A.; Furusawa, H.; Suenaga, A.; Okimoto, N.; Futatsugi, N.; Ebisuzaki, T. Nanoscale Hydrophobic Interaction and Nanobubble Nucleation. *Phys. Rev. Lett.* **2004**, *93*, 185701.
(21) Koishi, T.; Yasuoka, K.; Ebisuzaki, T.; Yoo, S.; Cheng, X. C. Large-Scale Molecular-Dynamics Simulation of Nanoscale Hydrophobic Interaction and Nanobubble Formation. *J. Chem. Phys.* **2005**, *123*, 204707.
(22) Bresme, F.; Oettel, M. On the Influence of Solute Polarizability on the Hydrophobic Interaction. *J. Phys.: Condens. Matter* **2007**, *19*, 413101.
(23) Bresme, F.; Faraudo, J. Orientational Transitions of Anisotropic Nanoparticles at Liquid-Liquid Interfaces. *J. Phys.: Condens. Matter* **2007**, *19*, 375110.
(24) Bresme, F.; Oettel, M. Nanoparticles at Fluid Interfaces. *J. Phys.: Condens. Matter* **2007**, *19*, 413101.
(25) Bresme, F.; Lehle, H.; Oettel, M. Solvent-Mediated Interactions Between Nanoparticles at Fluid Interfaces. *J. Chem. Phys.* **2009**, *130*, 214711.
(26) Lum, K.; Luzar, A. Pathway to surface-induced phase transition of a confined fluid. *Phys. Rev. E: Stat. Phys., Plasmas, Fluids, Relat. Interdiscip. Top.* **1997**, *56*, R6283−R6286.
(27) Wang, J.; Kudesia, S.; Bratko, S.; Luzar, A. Computational probe of cavitation events in protein systems. *Phys. Chem. Chem. Phys.* **2011**, *13*, 19902−19910.
(28) Vanzo, D.; Bratko, D.; Luzar, A. Dynamic Control of Nanopore Wetting in Water and Saline Solutions under an Electric Field. *J. Phys. Chem. B* **2015**, *119*, 8890−8899.
(29) Bresme, F.; Quirke, N. Computer Simulation Study of the Wetting Behavior and Line Tensions of Nanometer Size Particulates at a Liquid-Vapor Interface. *Phys. Rev. Lett.* **1998**, *80*, 3791.
(30) Wynveen, A.; Bresme, F. Interactions of Polarizable Media in Water: A Molecular Dynamics Approach. *J. Chem. Phys.* **2006**, *124*, 104502.
(31) Vanzo, D.; Bratko, D.; Luzar, A. Wettability of pristine and alkyl-functionalized graphane. *J. Chem. Phys.* **2012**, *137*, 034707.
(32) Ritchie, J. A.; Yazdi, J. S.; Bratko, D.; Luzar, A. Metastable Sessile Nanodroplets on Nanopatterned Surfaces. *J. Phys. Chem. C* **2012**, *116*, 8634−8641.
(33) Plimpton, S. Fast Parallel Algorithms for Short-Range Molecular Dynamics. *J. Comput. Phys.* **1995**, *117*, 1−19.
(34) Berendsen, H. J. C.; Grigera, J. R.; Stroatsma, T. P. The Missing Term in Effective Pair Potentials. *J. Phys. Chem.* **1987**, *91*, 6269−6271.
(35) Hockney, R. W.; Eastwood, J. W. *Computer Simulation Using Particles*; Adam Hilger: New York, 1989.
(36) Shinoda, W.; Shiga, M.; Mikami, M. Rapid Estimation of Elastic Constants by Molecular Dynamics Simulation Under Constant Stress. *Phys. Rev. B: Condens. Matter Mater. Phys.* **2004**, *69*, 134103.
(37) Giovambattista, N.; Debenedetti, P. G.; Rossky, P. J. Effect of Surface Polarity on Water Contact Angle and Interfacial Hydration Structure. *J. Phys. Chem. B* **2007**, *111*, 9581−9587.
(38) Giovambattista, N.; Rossky, P. J.; Debenedetti, P. G. Effect of Pressure on the Phase Behavior and Structure of Water Confined Between Nanoscale Hydrophobic and Hydrophilic Plates. *Phys. Rev. E* **2006**, *73*, 041604.
(39) Alencar, A. M.; Wolfe, E.; Buldyrev, S. V. Monte Carlo Simulation of Liquid Bridge Rupture: Application to Lung Physiology. *Phys. Rev. E* **2006**, *74*, 026311.
(40) Castrillón, S. R.-V.; Giovambattista, N.; Aksay, I. A.; Debenedetti, P. G. Structure and Energetics of Thin Film Water. *J. Phys. Chem. C* **2011**, *115*, 4624−4635.
(41) Starr, F. W.; Sciortino, F.; Stanley, H. S. Dynamics of Simulated Water under Pressure. *Phys. Rev. E: Stat. Phys., Plasmas, Fluids, Relat. Interdiscip. Top.* **1999**, *60*, 6757.
(42) Rowlinson, J. S.; Widom, B. *Molecular Theory of Capillarity*; Dover Publications: New York, 2002.
(43) Wang, J. Y.; Betelu, S.; Law, B. M. Line Tension Approaching a First-Order Wetting Transition: Experimental Results from Contact Angle Measurements. *Phys. Rev. E: Stat. Phys., Plasmas, Fluids, Relat. Interdiscip. Top.* **2001**, *63*, 031601.
(44) Cruz-Chu, E. R.; Aksimentiev, A.; Schulten, K. Water-Silica Force Field For Simulating Nanodevices. *J. Phys. Chem. B* **2006**, *110*, 21497−21508.
(45) Vega, C.; de Miguel, E. Surface Tension of the Most Popular Models of Water by Using the Test-Area Simulation Method. *J. Chem. Phys.* **2007**, *126*, 154707.
(46) Ismail, A. E.; Grest, G. S.; Stevens, M. J. Capillary Waves at the Liquid-Vapor Interface and the Surface Tension of Water. *J. Chem. Phys.* **2006**, *125*, 014702.
(47) Yang, S. H.; Nosonovsky, M.; Zhang, H.; Chung, K.-H. Nanoscale Water Capillary Bridges under Deeply Negative Pressure. *Chem. Phys. Lett.* **2008**, *451*, 88−92.

DOI: 10.1021/acs.jpcc.5b10377
J. Phys. Chem. C 2016, 120, 1597−1608

(48) Caupin, F.; Herbert, E.; Balibar, S.; Cole, M. W. Comment on "Nanoscale Water Capillary Bridges under Deeply Negative Pressure" [Chem. Phys. Lett. 451 (2008) 88]. *Chem. Phys. Lett.* **2008**, *463*, 283−285.
(49) Yang, S. H.; Nosonovsky, M.; Zhang, H.; Chung, K.-H. Response to the Comment on "Nanoscale Water Capillary Bridges under Deeply Negative Pressure" by Caupin et al. *Chem. Phys. Lett.* **2008**, *463*, 286−287.
(50) Wang, J.; Zeng, X. C. Computer Simulation of Liquid-Vapor Interfacial Tension: Lennard-Jones Fluid and Water Revisited. *J. Theor. Comput. Chem.* **2009**, *08*, 733−763.
(51) Law, B. M. Theory of Nucleated Wetting. *Phys. Rev. Lett.* **1994**, *72*, 1698−1701.
(52) Lazaridis, M. The Effects of Surface Diffusion and Line Tension on the Mechanism of Heterogeneous Nucleation. *J. Colloid Interface Sci.* **1993**, *155*, 386−391.
(53) Aleksandrov, A.; Toshev, B.; Scheludko, A. Nucleation from Supersaturated Water Vapors on N-Hexadecane: Temperature Dependence of Critical Supersaturation and Line Tension. *Langmuir* **1991**, *7*, 3211−3215.
(54) Macdowell, L. G.; Shen, V. K.; Errington, J. R. Nucleation and cavitation of spherical, cylindrical, and slablike droplets and bubbles in small systems. *J. Chem. Phys.* **2006**, *125*, 034705.
(55) de Gennes, P. G. Wetting: Statics and Dynamics. *Rev. Mod. Phys.* **1985**, *57*, 827−863.
(56) Dussan, E. B. On the Spreading of Liquids on Solid Surfaces: Static and Dynamic Contact Lines. *Annu. Rev. Fluid Mech.* **1979**, *11*, 371−400.

DOI: 10.1021/acs.jpcc.5b10377
J. Phys. Chem. C 2016, 120, 1597−1608